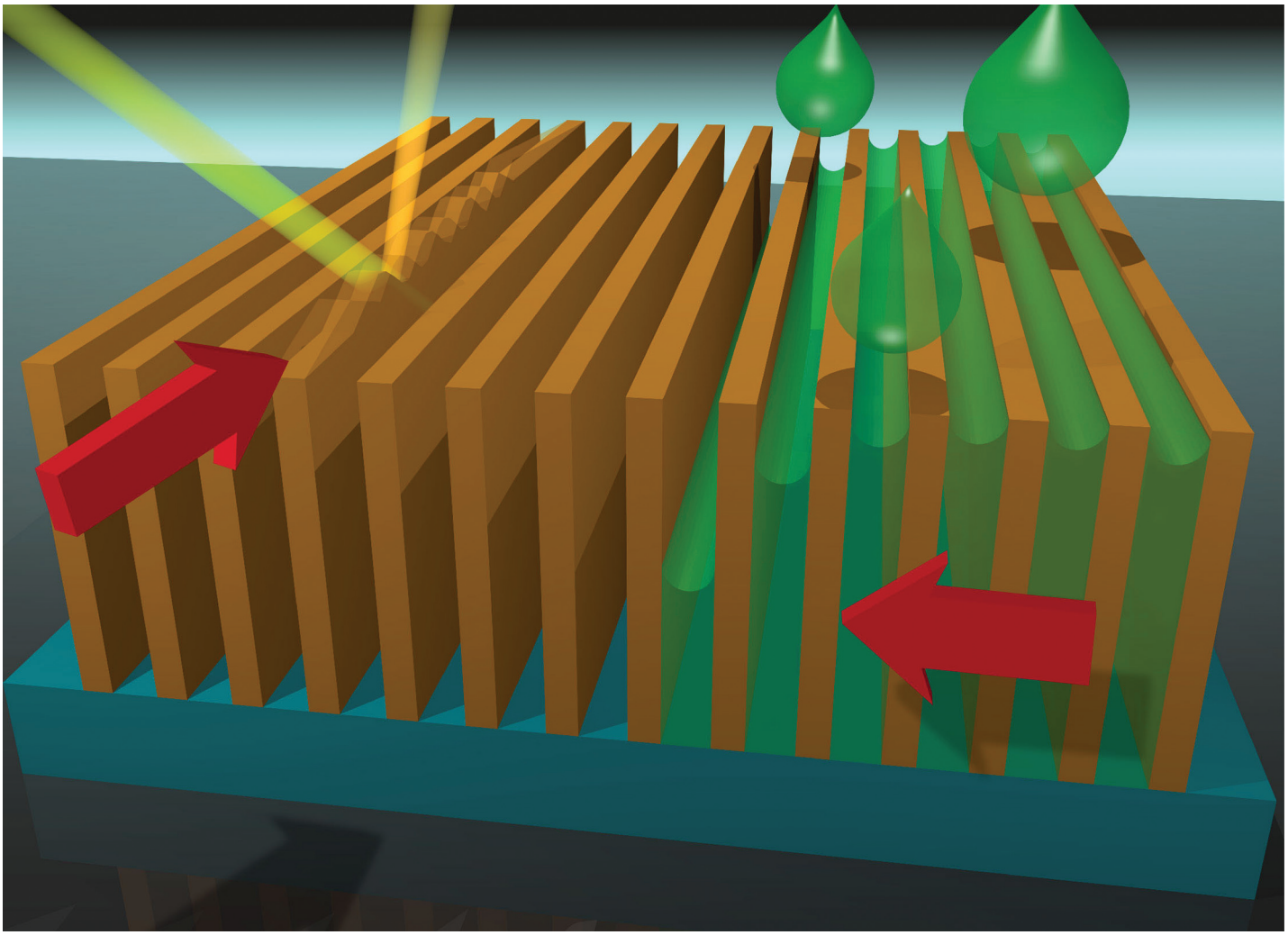

Showcasing research from the Max Planck Institute for Polymer Research, the University of Lille, The University Mohamed I, the University of Pennsylvania, the Catalan Institute of Nanoscience and Nanotechnology, and the University of Crete.

Directional elastic wave propagation in high-aspect-ratio photoresist gratings: liquid infiltration and aging

The vibrational modes in periodic high aspect-ratio nanowalls, assessed by Brillouin light scattering and finite element method calculations, reveal quantitative and qualitative differences with low aspect-ratio nanolines. These are attributed to the two-beam interference lithography fabrication and aging effects. The phononic behavior is drastically altered by changing the environment of the nanowalls, from a unidirectional guiding to an anisotropic propagation along two orthogonal directions in the liquid-infiltrated grating.

As featured in:

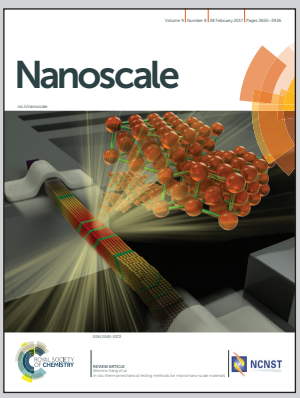

See G. Fytas *et al.*, *Nanoscale*, 2017, **9**, 2739.

ROYAL SOCIETY OF CHEMISTRY

rsc.li/nanoscale

Registered charity number: 207890

Nanoscale

PAPER

View Article Online
View Journal | View Issue

Cite this: *Nanoscale*, 2017, **9**, 2739

Directional elastic wave propagation in high-aspect-ratio photoresist gratings: liquid infiltration and aging†

E. Alonso-Redondo,[a] A. Gueddida,[b,c] J. Li,[d] B. Graczykowski,[e] C. M. Sotomayor Torres,[e,f] Y. Pennec,[b] S. Yang,[d] B. Djafari-Rouhani[b] and G. Fytas*[a,g]

Received 23rd October 2016,
Accepted 7th December 2016

DOI: 10.1039/c6nr08312a

rsc.li/nanoscale

Determination of the mechanical properties of nanostructured soft materials and their composites in a quantitative manner is of great importance to improve the fidelity in their fabrication and to enable the subsequent reliable utility. Here, we report on the characterization of the elastic and photoelastic parameters of a periodic array of nanowalls (grating) by the non-invasive Brillouin light scattering technique and finite element calculations. The resolved elastic vibrational modes in high and low aspect ratio nanowalls reveal quantitative and qualitative differences related to the two-beam interference lithography fabrication and subsequent aging under ambient conditions. The phononic properties, namely the dispersion relations, can be drastically altered by changing the surrounding material of the nanowalls. Here we demonstrate that liquid infiltration turns the phononic function from a single-direction phonon-guiding to an anisotropic propagation along the two orthogonal directions. The susceptibility of the phononic behavior to the infiltrating liquid can be of unusual benefits, such as sensing and alteration of the materials under confinement.

Thin and patterned polymer films with nanoscopic thicknesses are materials with growing interest, as the demand for miniaturization by the industry continues. Thin polymer structures are used in a variety of emerging applications including flexible electronics,[1,2] superhydrophobic coatings,[3,4] phononic crystals[5] and plasma etching masks.[6] The polymer nanostructures present advantages with respect to their hard (*e.g.* silicon, metal) counterparts as they can be transparent, biocompatible and low cost.[7] One dimensional (1D) gratings consisting of periodic arrays of nanowalls with a high aspect ratio (AR = height/width) are desired in many applications.[8] For example, as a plasma etching mask, high AR polymer nanowalls increase the etching resistance;[9] therefore the diffraction efficiency of the resulting grating is improved.[6] However, the increasing compliance also limits the maximum AR of nanowalls achievable, due to collapsing of the structures during fabrication or post-applications.[10]

The direct fabrication of high AR (>2) polymer gratings has been elusive by photo- and nanoimprint lithography using conventional polymers.[11] Organosilicate photoresists have enhanced the mechanical properties of the gratings, for the fabrication of stable ultrahigh AR gratings (up to 10) by interference lithography.[12] The mechanical properties of the resulting nanowalls differ from the bulk depending on the degree of polymerization, and post-exposure baking and rinsing processes. These nanowalls are amenable to buckling by boundary forces resulting from dissimilar expansion of the sample to the substrate.[13] Also, capillary forces during drying of patterned lithographic films from developer lead to pattern collapse if the AR is high or the material is mechanically weak.[14] The stability and mechanical properties of nanostructures are of paramount importance to guarantee their optimal performance. Therefore there is a requisite to develop methods to precisely determine the mechanical behavior of nanoscopic polymer structures.

The state-of-the-art methods for nanomechanic measurements are based on deformation,[15,16] or on acoustic wave

[a]*Max Planck Institute for Polymer Research, Ackermannweg 10, 55128 Mainz, Germany. E-mail: fytas@mpip-mainz.mpg.de*
[b]*Institut d'Electronique, de Microélectronique et de Nanotechnologie (IEMN), UMR-CNRS 8520, UFR de Physique, Université de Lille 1, 59655 Villeneuve d'Ascq, France*
[c]*LPMR, Département de Physique, Faculté des Sciences, Université Mohamed I, 60000 Oujda, Morocco*
[d]*Department of Materials Science and Engineering, University of Pennsylvania, 3231 Walnut Street, Philadelphia, PA 19104, USA*
[e]*Catalan Institute of Nanoscience and Nanotechnology (ICN2), CSIC and the Barcelona Institute of Science and Technology, Campus UAB, 08193 Bellaterra, Spain*
[f]*ICREA, Pg. Lluís Companys 23, 08010 Barcelona, Spain*
[g]*Department of Materials Science, University of Crete and IESL/FORTH, 71110 Heraklion, Greece*

†Electronic supplementary information (ESI) available. See DOI: 10.1039/c6nr08312a

propagation.[17,18] Both methods pose limitations: the former is destructive, while the latter requires complex sample preparation. Both assume a linear stress–strain relationship,[19] and cannot resolve the direction-dependent mechanical behaviors.[20] Yet, in the case of deformation tests, the estimation of the Young's modulus is based on the assumed value of the Poisson's ratio. The frequently employed atomic force microscopy (AFM) indentation technique suffers from drawbacks originating from small contact forces in the probe–sample interaction, and the influence of the rigid substrate.[21] In this context, Brillouin light scattering (BLS) emerges as a robust technique that provides an alternative for the non-invasive determination of the direction-dependent mechanical properties on the nanoscale, without complicated sample preparation. In BLS, the analysis of the spectral distribution of the scattered light by thermal phonons provides information about the mechanical properties of polymer thin films in their elastic response regime (GHz).[22] In the case of supported films, the influence of the supporting substrate is reliably predicted by theory.[23]

Here, we estimate the direction-dependent mechanical properties of high AR nanoscopic gratings using BLS. The recorded spectra (frequency and intensity) are a function of geometric, elastic and photoelastic parameters. Through finite element method (FEM) modeling we access the complete characterization of the 1D grating consisting of an array of nanowalls. Because the susceptibility of nanowall collapsing is dependent on the aspect ratio,[13,24] we evaluate the size-dependent fidelity on high AR and low AR nanowalls. The direction-dependence is assessed in both, pristine and buckled-defect gratings. Fundamental understanding of the mechanical properties of nanoscopic nanowalls will provide insights into how to improve the material performance, and realize the tuning of these sensitive materials by infiltrating a liquid in the interstices of the grating. The presence of periodicity in the sub-micrometer range invokes elastic wave (phonon) interactions in hypersonic frequencies that inevitably lead to deviations from the linear acoustic dispersion – frequency f *versus* wave vector $\mathbf{q}$ – that is a characteristic feature of homogeneous bulk materials. Recording of the rich dispersion $f(\mathbf{q})$ is necessary to unveil phononic behaviors that essentially determine the flow of the elastic energy in nanostructured materials. Therefore, in addition to the nanomechanic characterization, the phononic character of the grating is assessed in both pristine and liquid filled structures.

Results and discussion

1D gratings consisting of a periodic array of soft nanowalls were fabricated by two-beam interference lithography (Materials and methods) with two distinct AR = 11 (nanowalls, Fig. 1) and AR = 2 (nanolines).[25] In brief, the photoresist film was prepared from epoxy polyhedral oligomeric silsesquioxane (epoxy-POSS), a transparent organosilicate consisting of POSS molecules (the smallest silica particles) with covalently bonded epoxy groups suitable for photopolymerization. The spincoated film was exposed to a 532 nm-laser, and baked at 50 °C to crosslink the exposed regions. Then, the grating was developed in propylene glycol monomethyl ether acetate. The geometric parameters height h, width w and period a were determined by scanning electron microscopy (SEM) and are listed in Table 1. Nanowalls and nanolines are prepared directly on glass substrates, therefore the nanowalls are not in contact through any bottom layer.[26,27]

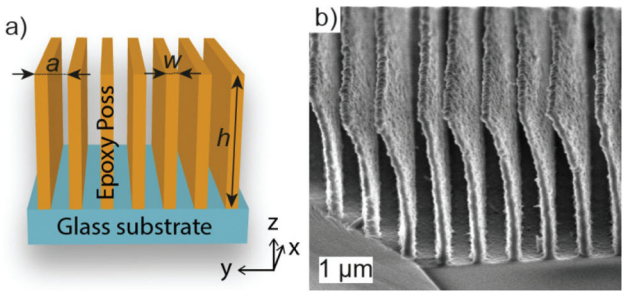

Fig. 1 Structure of the samples. (a) Schematic illustration of a 1D-grating with lattice constant a, width w, and height h along with the principal axes. (b) Scanning electron microscopy (SEM) images of nanowalls (AR = 11); the bending is due to the electron beam during imaging by SEM.

Table 1 Characteristic dimensions of the photoresist gratings[a]

Sample	h (nm)	w (nm)	AR	a (nm)	w/a
Nanolines	600	320	2	650	0.5
Nanowalls	2700	250	11	630	0.4

[a] Lattice constant (a), height (h), width (w), aspect ratio (h/w) and the width to lattice constant ratio (w/a).

High AR nanowalls

Direct measurements of the elastic properties in soft gratings are performed with the non-contact and non-destructive BLS technique. BLS spectroscopy is based on the photoelastic interaction of thermal hypersonic (GHz) elastic excitations with the probing laser beam. Thermal phonons interact with the photons to give rise to a momentum transfer manifested as frequency shifts in the recorded spectrum of the scattered light. The momentum transfer between the incident photon and an elastic single mode (phonon) is expressed as $\hbar\mathbf{q} = \hbar\mathbf{k}_s \pm \hbar\mathbf{k}_i$, where $\hbar\mathbf{k}_i$ and $\hbar\mathbf{k}_s$ are the momenta of the incident and scattered photons, respectively. The spectral Brillouin shift, f, depends on the direction and magnitude of the scattering wave vector $\mathbf{q}$ as described in the dispersion relation $f(\mathbf{q})$. For the transmission geometry (Fig. 2a), the magnitude of the wave vector is $q = 4\pi/\lambda_T \cdot \sin(\theta/2)$ (λ_T = 532 nm, θ is the scattering angle) and for the backscattering geometry (inset Fig. 2e) is $q = 4\pi/\lambda_{BS} \cdot \sin\alpha$ (λ_{BS} = 514.5 nm), where α is the angle of the beam to the normal of the substrate. Responsible for BLS in

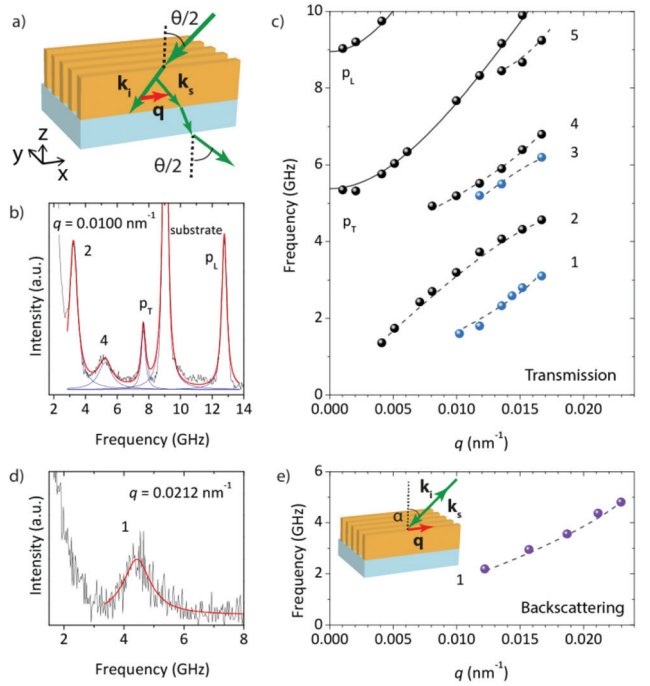

Fig. 2 Brillouin light scattering of high aspect ratio nanowalls. (a) Schematic of the BLS scattering geometry (transmission). $\mathbf{k}_i$ and $\mathbf{k}_s$ are the incident and scattered wave vectors respectively, oriented at an angle θ with respect to each other. $\mathbf{q}$ is the scattering wave vector along the nanowalls. (b) Experimental polarized (VV) BLS spectrum represented by a sum of Lorentzian shapes (blue and red solid lines). (c) Dispersion relation $f(\mathbf{q})$, acquired in VV (black circles) and VH (blue circles) polarizations. Solid lines denote the representation of p_L and p_t modes by using ESI eqn (1),† while the dashed lines are guide to the eye. (d) Experimental backscattering spectrum represented by a Lorentzian shape (red line). (e) Dispersion relation acquired in the backscattering geometry (inset) and HV polarization; dashed line is guide to the eye.

transmission and backscattering geometries is the photoelastic and surface ripple mechanisms, respectively. The ripple mechanism –weak in transparent materials–[28,29] is enhanced in this transparent material by a thin (~15 nm) aluminum coat, which results in a weak blue shift (<3%) of the phonon frequencies due to structure stiffening, as confirmed by FEM calculations. In the transmission geometry, the incident light is polarized vertically (V) to the scattering plane *xz* (Fig. 2a). The polarized spectra were recorded with vertical (V) polarization, while the depolarized spectra were recorded with horizontal (H) polarization (in the *xz* plane). In the back-scattering experiment, the incident light is horizontally polarized, and the collected light is vertically polarized (HV). Polarized and depolarized light carry distinct information about longitudinal or transverse displacement modes, respectively. The dispersion $f(\mathbf{q})$ was recorded for phonon propagation along the nanowalls (*x*-axis, Fig. 2a) because along the periodicity direction (*y*-axis) the strong diffracted beams obscure the BLS signal in the transmission geometry. The periodicity effect (p_L and p_T branches) is discussed in the ESI.†

The dispersion plot (Fig. 2c) consists of five branches (1–5) related to the different elastic excitations within the photoresist gratings, along the nanowalls. The recorded spectra in the transmission geometry consist of many peaks (representative spectrum shown in Fig. 2b), and in the backscattering geometry a single phonon was observed (Fig. 2d). The dispersion relation $f(\mathbf{q})$ shown in Fig. 2c consists of a collection of branches acquired in VV polarization (black) and VH polarization (blue). Branch 1 in Fig. 2e was acquired with HV polarization in the backscattering geometry. We note that a single sample was used to record the dispersion in each case; the reproducibility (within 1%) was proven using an additional sample. The nature of the observed modes is being disclosed by the theoretical representation of the full BLS spectrum.[5]

We utilize FEM analysis (Materials and methods) to calculate the dispersion curves of elastic waves propagating along the nanowalls. Many modes are anticipated due to the finite size of the nanowalls and their attachment to a quasi-rigid substrate; however, only a discrete number of modes were observed in the experiment. To filter the modes that contribute strongly to the BLS intensity, we use the band sorting method (ESI and Fig. S1†) and the photoelastic coupling between the probing light and the sorted elastic modes.[30] The dielectric tensor ε_{jk} at any given point is modulated by the elastic wave due to the strain tensor S_{lm}: $\delta\varepsilon_{jk} = P_{jklm}\, S_{lm}$, where P_{jklm} is the photoelastic (Pockels) tensor. In isotropic homogeneous media, only two photoelastic constants describe the materials, in Voigt notation P_{11} (= P_{1111}) and P_{12} (= P_{1122}).[31] The BLS intensity is given by $I = |E^s|^2 \propto \left|\frac{1}{2\pi f}\int_V e^{i\vec{q}\vec{r}} \sum_{klm} P_{jklm} S_{lm} E^0 \mathrm{d}V\right|^2$, where E^0 and E^S are the incident and scattered electric fields, respectively, V is the scattering volume and i is the imaginary number. In our particular case where the propagation is along x ($\vec{r} = (1, 0, 0)$), the BLS intensities in VV and VH polarizations are[32]

$$I_{VV} \propto \left|\frac{1}{2\pi f}\int_V e^{iqx}\left(P_{12}\partial_x u_x + P_{11}\partial_y u_y + P_{12}\partial_z u_z\right)E^0 \mathrm{d}V\right|^2 \quad (1)$$

$$I_{VH} \propto \left|\frac{1}{2\pi f}\int_V e^{iqx}\frac{P_{11}-P_{12}}{2}\left[\cos\frac{\theta}{2}\left(\partial_x u_y + \partial_y u_x\right) + \sin\frac{\theta}{2}\left(\partial_y u_z + \partial_z u_y\right)\right]E^0 \mathrm{d}V\right|^2 \quad (2)$$

where u_i is the displacement and ∂_j denotes a partial derivative along the j-th direction. The selection rules in eqn (1) and (2) allow only a few modes to contribute to the BLS intensity in each polarization (Fig. 3a and b). The theoretical spectra were convoluted with the instrumental width (~0.3 GHz). The excess of broadening in the experimental spectrum is due to additional damping because of phonon scattering and secondary relaxations in the glassy epoxy. The nanowall elastic and photoelastic parameters (in Table 2) are then obtained from the unique theoretical description of the full experiment (dispersion and peak intensities).

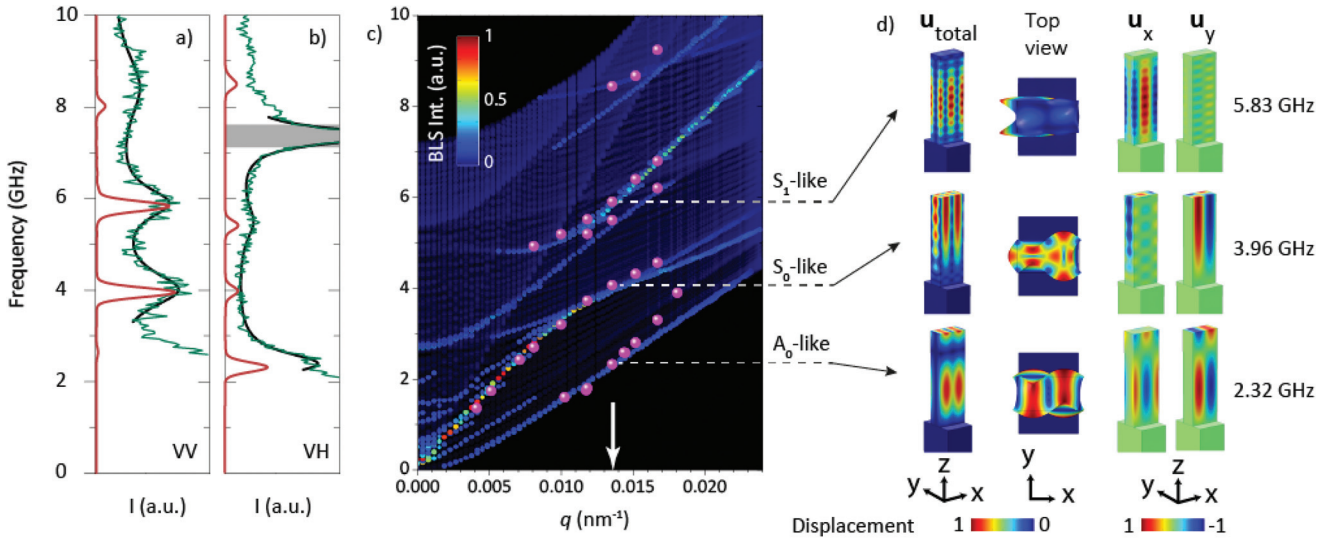

Fig. 3 High aspect ratio nanowalls. (a, b) Experimental (green) and computed (red) spectrum at q = 0.0135 nm^{-1} in VV and VH polarization. The experimental spectra have been represented by a sum of Lorentzian shapes (black). The shaded region in (b) corresponds to the scattering by the glass substrate. (c) Computed BLS intensity (VV + VH polarizations) and experimental (pink circles) phononic band diagram. The arrow marks the wavenumber of the spectra in (a, b). (d) Normalized total ($\mathbf{u}_{total}$) and selected displacement fields along the x ($\mathbf{u}_x$) and y ($\mathbf{u}_y$) directions of a nanowall slice (tilted, see *xyz* axes), at q = 0.0135 nm^{-1} and three frequencies as indicated in the plot. For visualization purposes, the total displacement has been exaggerated, and the nanowall AR is not to scale.

Table 2 Values of the physical quantities used in the theoretical calculations[a]

Parameter	Nanowalls	Nanolines	Glass substrate	Cargille	PDMS
ρ (kg m^{-3})	1190	1190	2200	1000	965
c_L (m s^{-1})	2620	2950	5660	1670	1000
c_T (m s^{-1})	1350	1450	3390	0	0
ν	0.32	0.34	0.22		
E (GPa)	5.29	6.20	617		
P_{11}/P_{12}	0.100	0.667			

[a] Density (ρ), longitudinal (c_L) and transverse (c_T) sound velocities, Poisson's ratio (ν), Young's modulus (E) and photoelastic coefficients ratio (P_{11}/P_{12}).

Fig. 3c displays the theoretical BLS intensity ($I_{VV} + I_{VH}$) dispersion relation. The bands with a sufficiently large BLS intensity are colored, while the bands with zero intensity (dark blue) are set to a certain transparency for visualization purposes. A thorough inspection of the dispersion plot (Fig. 3c) reveals that the experimental points can be satisfactorily described by the Lamb modes of an infinite plate of the same wall thickness, w (Fig. S2†). Lamb modes are classified as A_n and S_n, with antisymmetric and symmetric displacements of the plate free surfaces from their mid-plane, respectively. Based on the displacement field, A_n modes are observed in VH (Fig. 3b, eqn (2)), while S_n modes are observed in VV (Fig. 3a, eqn (1)) polarization. The fundamental modes A_0 (flexural) and S_0 (extensional) are the most important ones since they carry a large fraction of the elastic energy and have no low cut-off frequency at q = 0 (Fig. 3c). The cut-off frequency of higher order modes is $f = mc/2w$, where m is a positive integer, and c is either the epoxy's transverse velocity for even A_n and odd S_n modes, or the epoxy's longitudinal velocity for odd A_n and even S_n modes. The dependence of the fundamental modes on the transverse c_T and longitudinal c_L velocities of sound in epoxy is related to their symmetry and wave vector. For instance, the S_0-like mode is sensitive to the variation of c_T and not too much to c_L, whereas the S_1-like mode is sensitive to the variation of c_L and becomes sensitive also to c_T when the wave vector increases. A more quantitative evaluation of these dependences is discussed in the ESI (see Fig. S3†). In our work, the band structure has been calculated for several choices of these velocities. The best comparison with experiments is obtained for the c_L and c_T values listed in Table 2 with a variance about 4% and 10%, respectively. The elastic parameters listed in Table 2 reveal bulk-polymer-like behavior of pristine high AR nanowalls as both the Poisson ratio (0.32) and the longitudinal sound velocity (2620 m s^{-1}) are values typical of glassy polymers. Access to exactly the same bulk material forming the gratings is not possible, since the fabrication involves a process of crosslinking by an interference pattern of variable intensities, and post-exposure baking and developing that affects the final properties.[33] Hence, the non-destructive *in situ* characterization of the grating is crucial.

The observed modes 1–5 shown in Fig. 2c are identified as A_0, S_0, A_1, S_1 and S_2 (Fig. 3c), respectively. The displacement fields of some of the modes that contribute to the BLS intensity are displayed in Fig. 3d. These modes can be understood as guided modes along the x direction, and stationary in the y and z directions. At low q values ($<2\pi/w \sim 0.026$ nm^{-1}), the A_0-like mode (active in VH and HV polarizations) is dominated

by the transverse displacement u_y, while the S_0-like mode (active in VV) is prevailed by the longitudinal u_x displacement. At high q values, the wavelength of the phonon is shorter than the wall thickness, and the A_0 and S_0 modes propagate on the vertical free surfaces of the walls with the speed of a Rayleigh wave of epoxy. Higher harmonics, corresponding to the stationary waves along the height of the nanowall with their oscillations in the z-axis, contribute little to the BLS spectra (blue-transparent lines in Fig. 3c). These modes become more important with the decrease in the grating AR, and indeed their intensity is stronger in nanolines (Fig. 4g).

Aging effects

Polymer gratings are amenable to age by factors such as humidity, stress and temperature.[13,19,34,35] Since one of our goals is to tune the elastic properties of nanowalls by liquid infiltration, the study of possible shape deformation of the gratings under wet conditions is relevant. Nanowalls stored in the lab for a few months –under ambient temperature (≈23 °C) and humidity– are buckled (Fig. 4a). It has been reported that the nanowalls exposed to humidity absorb water and swell.[36] Because the nanowalls are attached to a quasi-rigid substrate, residual stress along the lamina is created. When the critical stress S^* is reached –depending on the nanowall aspect ratio–, straight nanowalls form wavy patterns.[19]

Since the elastic vibrations of the straight nanowalls can be described effectively by an infinite plate, the BLS intensities of the buckled structures are computed for the infinite plate instead of the finite nanowalls. The theoretical BLS intensities at several q values are displayed for three values of the amplitude (δ) and the period (d) of the wavy patterns (inset to Fig. 4a) and are displayed in Fig. 4b and c, respectively. The blue lines are for d = 8400 nm and δ = 646 nm (observed values by SEM) and the green lines denote the spectral shape

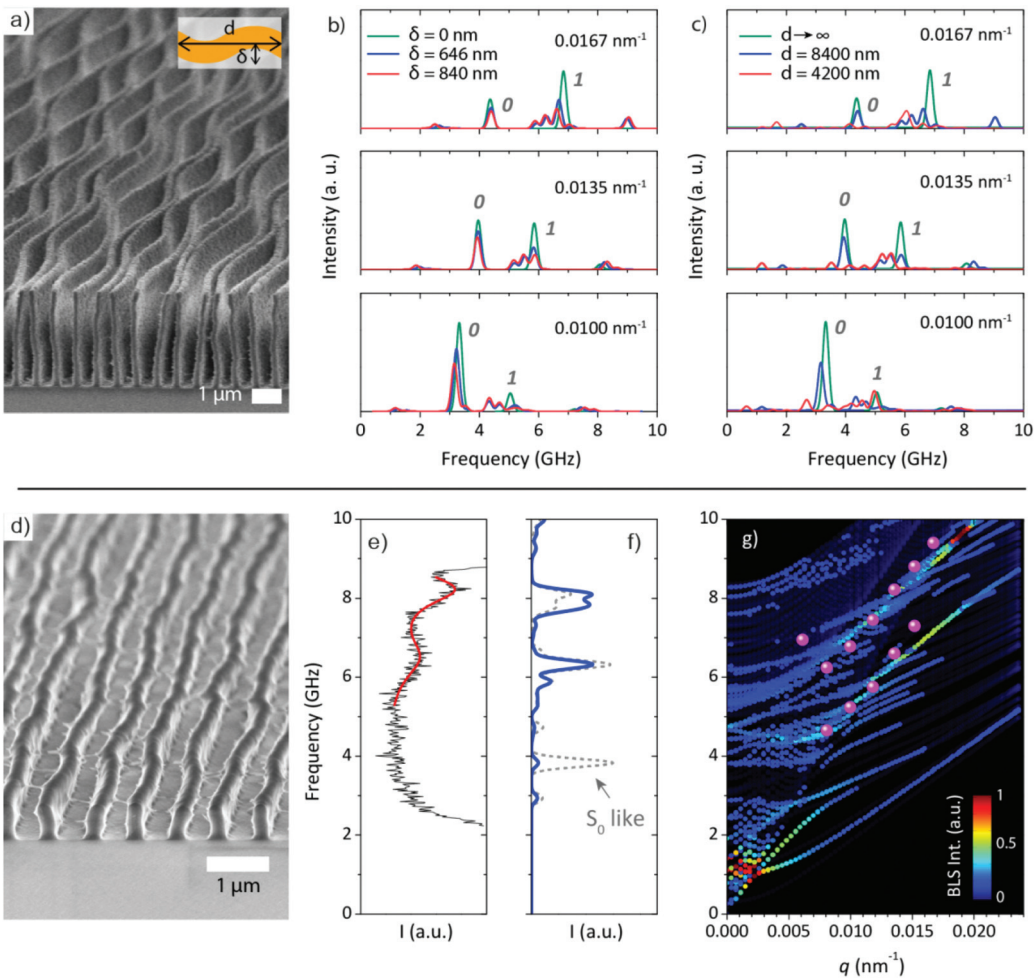

Fig. 4 Aging effects. (a) Cross sectional SEM micrograph of nanowalls. (b, c) Computed VV BLS intensity of a buckled infinite plate. The amplitude (δ) and period (d) of the ondulation is varied around its mean value 646 nm and 8400 nm in (b) and (c), respectively (blue lines). The parameters were fixed to d = 8400 nm in (b) and δ = 646 nm in (c). The intensity spectrum of a straight nanowall is shown (green lines); the peaks identified as **0** and **1** correspond to the S_0-like and S_1-like modes, respectively. (d) Cross sectional SEM micrograph of nanolines. (e) Experimental (VV polarization) and (f) computed spectrum at q = 0.0135 nm^{-1} in nanolines. In (f) the theoretical spectra are calculated using P_{11}/P_{12} = 0.67 (blue line) and (c) P_{11}/P_{12} = 0.10 (grey dashed line). (g) Computed BLS intensity and experimental (pink circles) phononic band diagram of the nanolines in VV polarization.

for the straight plate (δ = 0 nm or $d \rightarrow \infty$). In general, a variation of either d or δ results in a diminution of the BLS intensities accompanied by a slight red-shift relative to the straight plate case; to observe a significant red-shift, δ/d must be unrealistically small. As this zig-zag structure does not display a symmetry plane, more modes (than only S_0-like and S_1-like) can be involved in the scattering process. The results remain similar to the straight nanowalls as far as the ratio δ/d is small, while upon increasing δ/d more modes appear in the vibration spectrum. Therefore, a moderated buckling does not strongly affect the phonon propagation along the nanowalls.[37]

The apparent touching of the buckled nanowalls (Fig. 4a) could, in principle, alter the dispersion relation, and the phonon-guiding character. To precisely evaluate the influence of contact between walls, the dispersion relation for two walls touching by their tops was computed. No significant changes in the dispersion are found for one-point contact, or 1/4 of the nanowall height h (Fig. S4†). For a touching portion larger than $h/2$, there are significant changes in the dispersion; the formed pseudo-plate behaves as a Lamb plate of a $2w$ thickness. Nevertheless, the latter scenario is highly unrealistic and is disregarded. Consequently, touching of the nanowalls is not expected to alter the phononic properties. However, the experimental dispersion relation of the aged gratings reveals changes at high q values (or short sizes) and the observed disparity deviation is ascribed to morphological issues due to fabrication (see the ESI and Fig. S4, S5 and S6†). In this context it is worth mentioning that in previous backscattering BLS studies on polymer nanolines the effect of the trapezoidal shape was not considered in the numerical calculations.[38]

In order to test the role of the nanowall height on the buckling effect, we measured the dispersion of short AR (= 2) nanolines by BLS. In contrast to the nanowalls, short AR nanolines seem to be robust against buckling and there is no significant deformation (Fig. 4d) when aged under the same conditions as the nanowalls. Assuming that $S^* \times (\mathrm{AR})^2$ is constant for the same material,[19] the critical compression stress S^* in the case of nanolines should be ≈30 times higher than that of the nanowalls, in agreement with the absence of significant deformation in Fig. 4d. Thus, nanolines can accommodate higher stress than nanowalls. To qualitatively capture the band structure shown in Fig. 4g, faster sound velocities and hence higher Young's modulus of nanolines are necessary compared to those for nanowalls (Table 2). This is in line with the expected increase of bending stiffness and the compressive residual stress of short AR nanolines.[11,39] The disparity of the mechanical strength (~15%) in the two photoresist gratings fabricated by using the same original material clearly indicates the necessity of non-destructive metrology, in particular for nanostructures. And this is not restricted to a single physical property (Table 2).

The experimental dispersion of nanolines can still be captured by the guided Lamb modes of an infinite plate of the same width w (Fig. S1†), in spite of their small AR. However, the suppression of the extensional S_0 mode in the nanoline spectrum is remarkable (Fig. 4f) in view of the strong intensity of S_0 in high AR nanowalls (Fig. 3a). The justification of the S_0 suppression involves a photoelastic coefficient ratio of P_{11}/P_{12} higher than that in the nanowall case (0.67 *vs.* 0.10 in Table 2), despite being fabricated from the same original material. A possible reason for this elasto-optic modification could be related to the variation of the epoxy crosslinking characteristics, as a consequence of the sinusoidal interference light intensity, and the longer crosslinking times for short nanolines.[12] As P_{11} relates to displacements parallel to the polarization direction (y-axis), *i.e.* flexural modes, a stronger crosslinked polymeric matrix could accommodate an increase of P_{11}. While the photoelastic coefficients are well defined for crystalline materials,[40] in the case of polymers subtle local structural changes can impart these coefficients. Again this disparity emphasizes the importance of material characterization on different length scales.

Liquid filled gratings

Based on the displacement field of the vibration modes shown in Fig. 3d, the strain is localized inside the nanowall volume, while the substrate is essentially unstrained. In order to examine the phonon confinement along the buckled nanowalls, we recorded the dispersion relation with different orientations of **q** with respect to the wall direction, as illustrated in the inset to Fig. 5. The superposition of the modes 1, 2 and 4 when their frequencies are plotted as a function of the projected q_x (= $q \cdot \cos\varphi$) evidences the guidance of the elastic excitations along the nanowalls. In fact, the computed density of states at several angles φ (Fig. S7†) supports the experimental finding. This is an advantage when utilizing nanowalls as hosts for liquids; we emphasize that the main discrepancies between the empty and the liquid-filled nanowalls are not due to buckling, but entirely to the filling liquid.

The phononic behavior of high AR gratings is expected to be significantly altered upon the presence of a different

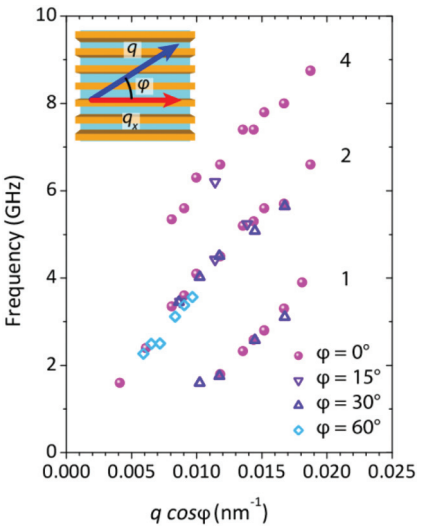

Fig. 5 Phonon guiding. Dispersion relation as a function of the projected q_x along the nanowalls. The inset sketches the nanowall top-view, indicating that the direction of q is tilted by an angle φ.

environment (*i.e.* liquid). We infiltrated the gratings with a refractive index matched liquid (*Cargille Laboratories*) that partially suppresses the diffracted beams in the transmission geometry. In this case, it is possible to record the phonon propagation across the nanowalls (y direction). The infiltration of the grating with a liquid allows the propagation of the longitudinal acoustic wave along and across the nanowalls. Fig. 6a displays the theoretical and experimental dispersion relation for propagation across the nanowalls (where the displacement mainly has u_y and u_z components) of Cargille-filled nanowalls. In this case, the grating behaves as a 1D phononic crystal[5] for longitudinal waves across the walls with the experimental points falling into the reduced 3rd and 4th Brillouin zone. There is a deviation from the bulk-like behavior (linear dispersion) caused by the periodicity in the sub micrometer range. The branches with the highest BLS intensities in Fig. 6a relate to the well-known folded acoustic branches of an infinite 1D phononic crystal. Between these branches, additional branches with little contribution to BLS (dark blue dots in Fig. 6a) correspond to stationary waves along the z-axis as a consequence of the finite size of the grating. The dispersion relation across the nanowalls (y axis) is qualitatively different from that along nanowalls (x axis, Fig. 6b) for which no band gap is predicted. However, the experimental dispersion could look similar (Fig. S8†) in view of the similar effective sound velocities in parallel ($c_{\mathrm{eff},x}$ = 2130 m s^{-1}) and perpendicular ($c_{\mathrm{eff},y}$ = 1880 m s^{-1}) to the walls. In this case, the phonon guiding evidenced in Fig. 5 is not apparent, and was confirmed by measurements (not shown here) at different orientation angles φ.

The dispersion relation along the nanowalls (x-axis) is distinctly different in the two cases of empty (Fig. 3c) and filled (Fig. 6b) gratings. While the former displays multiple branches corresponding to the propagation of phonons along the nanowalls, the dispersion relation of the latter has two branches of an S-like character. The experiment captures only the upper one (Fig. 6b), probably because the lower branch is obscured by the Rayleigh peak in the spectra. The higher orders contribute weakly to the BLS intensity. Note that in the FEM calculations of the infiltrated grating the effect of buckling was not simulated because first, the wavy patterns are random and second, the wavelength of the wavy patterns (d) is much longer in comparison with the phonon wavelength; these two factors cannot lead to an observable phononic effect.[41] Hence, the simulations were performed with straight nanowalls. The elastic and photoelastic parameters needed for the theoretical modelling are the same in the filled and empty gratings. The newly introduced parameter is the photoelastic coefficient for the liquid P = 4, which adopts a value higher than that in the epoxy.

In order to verify the sensitivity of the grating to different infiltrating liquids, we filled a second sample of nanowalls with PDMS. In contrast to the previous case, the dispersion curves (Fig. 6c) contained an almost flat branch around 5 GHz, observed also in other periodic structures infiltrated with PDMS.[22] It is supposed that a very thin solidified layer of PDMS is formed under confinement. The flat branch in Fig. 6c can be rationalized if we assume that PDMS forms a solid layer in contact to the epoxy nanowalls of 10 nm thickness and a transverse sound velocity of $c_{\mathrm{T,layer}}$ = 250 m s^{-1}. This theoretical flat branch in Fig. 6c obtained in this way is associated with a strong displacement field in the solid PDMS layer. The susceptibility of the guided modes along nanowalls to the infiltrating liquid can be of unusual benefits: both sensing and alteration of the materials under confinement.[42]

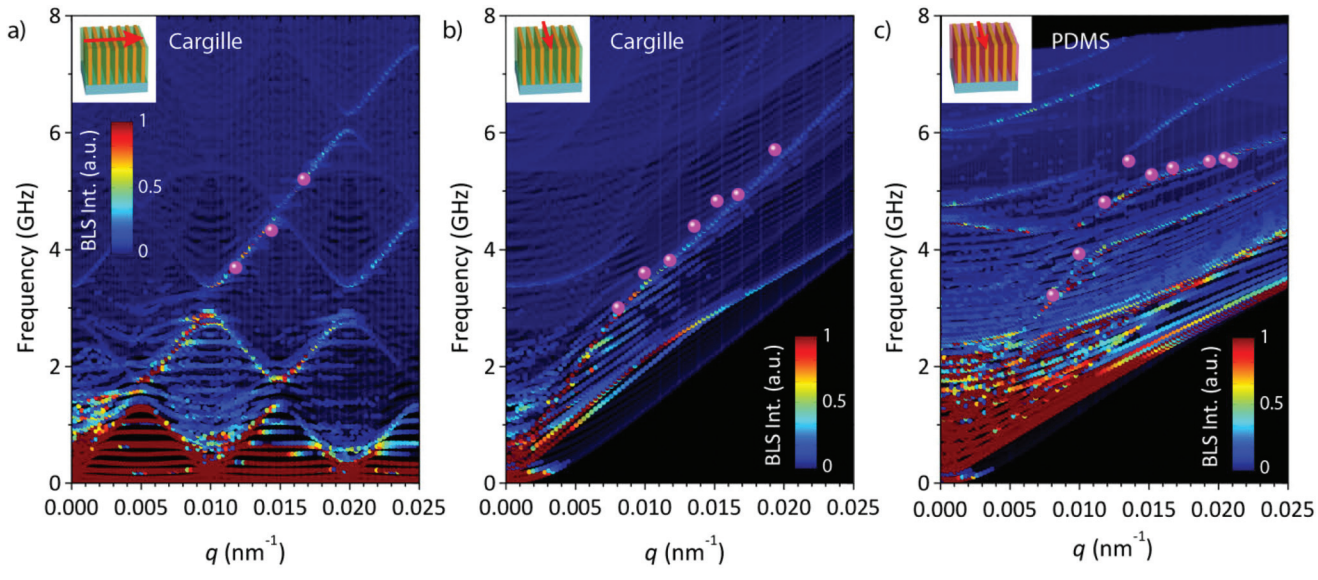

Fig. 6 Infiltration. (a, b) Theoretical and experimental (pink dots) phononic dispersion relations (a) across and (b) along the high aspect ratio nanowalls infiltrated with the *Cargille* liquid. (c) Theoretical and experimental phononic dispersion relations along PDMS-infiltrated nanowalls. PDMS is assumed to form a thin (10 nm) solid ($c_{\mathrm{T,layer}}$ = 250 m s^{-1}) layer around the nanowalls.

Conclusions

We have studied the elastic excitations of 1D epoxy-POSS gratings using the BLS normal to the periodicity direction for two different ARs. Full FEM calculations yield the elastic and photoelastic parameters of the structure that are dependent on the fabrication conditions and aging. We demonstrated that the propagation of elastic waves along the epoxy nanowalls is preserved when the grating is in air despite the buckling defects present in the high AR nanowalls after aging. The liquid infiltration activates the propagation across the nanowalls. The recorded dispersion along the two main orthogonal directions (x and y) is distinct, revealing anisotropy in the phonon propagation. The nanowall gratings are likely to be suitable not only as hosts for liquids but also as nano-building blocks towards three-dimensional architectured materials.[43] Specifically, the assembly of building blocks on different length scales could lead to phonon filtering applications for stiffer structures.[44–46]

Materials and methods

Fabrication of nano-gratings

The soft gratings were fabricated by two-beam interference lithography according to the procedure described in ref. 12. In brief, the photoresist film was prepared from 50–70 wt% of epoxy polyhedral oligomeric silsesquioxane (epoxy-POSS, EP0408 from *Hybrid Plastics*) and 0.9 wt% (relative to the mass of epoxy-POSS) Irgacure 261 (visible photoacid generator, PAG, *Ciba Specialty Chemicals*). The exposed regions were crosslinked by baking at 50 °C for 35 s, followed by development in propylene glycol monomethyl ether acetate (PGMEA, *Sigma-Aldrich*) for 30 min.[12] To prevent the pattern collapse of the high aspect ratio nanolines, we rinsed the sample in isopropanol (IPA, *Sigma-Aldrich*) for 30 min, followed by drying in CO_2 supercritical point dryer (SAMDRI®-PVT-3D, *Tousimis*). The incident angles of the beams determine the periodicity and the height of the nanolines (*i.e.* film thickness) could be fine-tuned by the spin coating speed. Here, we investigated two of them, AR = h/w = 2 (nanolines) and 11 (nanowalls).

Scanning electron microscopy

The morphology and dimensions of the nanowalls and nanolines were characterized by using a scanning electron microscope (SEM, *LEO Gemini* 1530) at 0.7 kV.

Brillouin light scattering

BLS is a non-invasive technique which utilizes the scattering of an incident probing laser beam from thermally activated density fluctuations (phonons) in transparent materials along a certain direction. In the transmission geometry, the probing wave vector orientation with respect to the nanowalls is selected with the scattering geometry, and its wavenumber $q = 4\pi/\lambda\sin(\theta/2)$ is dependent on the wavelength of the probing beam λ = 532 nm and the scattering angle θ for propagation parallel to the substrate plane. The BLS spectrum consists of a family of frequency doublets at GHz frequencies, resolved by using a tandem Fabry-Perót interferometer (*JRS Instruments*). In the backscattering (BS) geometry, the wavenumber $q = 4\pi/\lambda_{BS}\sin(\alpha)$ (λ_{BS} = 514.5 nm) depends on the angle of incidence α respect to the normal of the film. The BLS spectra are represented by a sum of Lorentzian shapes; the error in the peak position is about ±0.05 GHz (<1%).

Theoretical modeling

The dispersion curves $f(\mathbf{q})$ of the nanowalls are obtained by solving the elasticity equations of motion by using the finite element method (FEM), by means of the software *Comsol Multiphysics*. Due to the periodicity of the structure along the y direction, the problem is solved in one unit cell by assuming periodic boundary conditions at the limits of the unit cell. Free stress boundary conditions are used at the surfaces of the ridge which are in contact with vacuum whereas fixed boundary conditions are used at the bottom surface of the glass substrate (assumed to be of finite thickness). In the liquid-filled gratings, the boundary conditions at the liquid/solid interface are continuous for the normal stress and the normal displacement, given by $\nabla p = \rho(2\pi f)^2 u$. From the knowledge of the eigenvalues and eigenvectors of the structure, one can calculate the BLS spectra based on eqn (1) and (2). The calculations were performed using the parameters in Table 2; otherwise is stated. The sensitivity of the peak position of the modes in the theoretical spectra has a complex dependence on the elastic parameters and the wavenumber q, and is illustrated in ESI Fig. S6.† The theoretical spectra are compared with experiments by allowing the epoxy's acoustic velocities c_L and c_T to change by 10% and 4%, respectively, with respect to the best agreement.

Acknowledgements

A. G. and B. D. R. thank E. H. El Boudouti for several helpful discussions about the theoretical calculations of the BLS spectra. E. A. R. and G. F. thank D. Schneider for his support in the initial stage of the BLS study and acknowledge the support from ERC SuPro 340391 and ERC SmartPhon 694977, respectively. S. Y. acknowledges the support by the National Science Foundation (NSF), Grant #CMMI-0900468. B. G. and C. M. S. T. gratefully acknowledge support from the EC project MERGING (GA nr. 309150), the Spanish project PHENTOM (FIS 2015-70862P) and the Severo Ochoa Program (MINECO, Grant SEV-2013-0295). B. G. acknowledges the Alexander von Humboldt foundation for support.

References

1 Z. B. Wang, M. G. Helander, J. Qiu, D. P. Puzzo, M. T. Greiner, Z. M. Hudson, S. Wang, Z. W. Liu and Z. H. Lu, *Nat. Photonics*, 2011, **5**(12), 753–757.
2 H. Kang, S. Jung, S. Jeong, G. Kim and K. Lee, *Nat. Commun.*, 2015, **6**, 6503.

3 P. Papadopoulos, X. Deng, L. Mammen, D. M. Drotlef, G. Battagliarin, C. Li, K. Mullen, K. Landfester, A. del Campo, H. J. Butt and D. Vollmer, *Langmuir*, 2012, **28**(22), 8392–8398.
4 S. Neuhaus, N. D. Spencer and C. Padeste, *ACS Appl. Mater. Interfaces*, 2012, **4**(1), 123–130.
5 D. Schneider, F. Liaqat, E. H. El Boudouti, Y. El Hassouani, B. Djafari-Rouhani, W. Tremel, H. J. Butt and G. Fytas, *Nano Lett.*, 2012, **12**(6), 3101–3108.
6 C. David, J. Bruder, T. Rohbeck, C. Grünzweig, C. Kottler, A. Diaz, O. Bunk and F. Pfeiffer, *Microelectron. Eng.*, 2007, **84**(5–8), 1172–1177.
7 B. Graczykowski, M. Sledzinska, N. Kehagias, F. Alzina, J. S. Reparaz and C. M. Sotomayor Torres, *Appl. Phys. Lett.*, 2014, **104**, 123108.
8 Y. Choi, H. Jeon and S. Kim, *Lab Chip*, 2015, **15**, 642.
9 Y.-C. Tseng, A. U. Mane, J. W. Elam and S. B. Darling, *Adv. Mater.*, 2012, **24**, 2608–2613.
10 Y. Zhang, C.-W. Lo, J. A. Taylor and S. Yang, *Langmuir*, 2006, **22**, 8595–8601.
11 V. Kalima, S. Siitonen, P. Karvinen, M. Suvanto, M. Kuittinen and T. T. Pakkanen, *J. Micromech. Microeng.*, 2008, **18**(2), 025020.
12 J. Li and S. Yang, *Microelectron. Eng.*, 2014, **128**, 7–11.
13 J. Li, Y. Cho, I.-S. Choi and S. Yang, *Adv. Funct. Mater.*, 2014, **24**(16), 2361–2366.
14 S. P. Delcambre, R. A. Riggleman, J. J. de Pablo and P. F. Nealey, *Soft Matter*, 2010, **6**(11), 2475.
15 Y. Liu, Y.-C. Chen, S. Hutchens, J. Lawrence, T. Emrick and A. J. Crosby, *Macromolecules*, 2015, **48**(18), 6534–6540.
16 P. A. O'Connell and G. B. McKenna, *Science*, 2005, **307**, 1760–1763.
17 A. Ayouch, X. Dieudonné, G. Vaudel, H. Piombini, K. Vallé, V. Gusev, P. Belleville and P. E. Ruello, *ACS Nano*, 2012, **6**(12), 10614–10621.
18 C. L. Poyser, T. Czerniuk, A. Akimov, B. T. Diroll, E. A. Gaulding, A. S. Salasyuk, A. J. Kent, D. R. Yakovlev, M. Bayer and C. B. Murray, *ACS Nano*, 2016, **10**(1), 1163–1169.
19 V. R. Tirumala, C. M. Stafford, L. E. Ocola, J. F. Douglas and L. Mahadevan, *Nano Lett.*, 2012, **12**(3), 1516–1521.
20 D. Schneider, N. Gomopoulos, C. y. Koh, P. Papadopoulos, F. Kremer, E. L. Thomas and G. Fytas, *Nat. Mater.*, 2016, **15**, 1079.
21 M. Paven, R. Fuchs, T. Yakabe, D. Vollmer, M. Kappl, A. N. Itakura and H.-J. Butt, *Adv. Funct. Mater.*, 2016, **26**(27), 4914–4922.
22 A. Sato, Y. Pennec, N. Shingne, T. Thurn-Albrecht, W. Knoll, M. Steinhart, B. Djafari-Rouhani and G. Fytas, *ACS Nano*, 2010, **4**(6), 3471–3481.
23 W. Cheng, R. Sainidou, P. Burgardt, N. Stefanou, A. Kiyanova, M. Efremov, G. Fytas and P. F. Nealey, *Macromolecules*, 2007, **40**(20), 7283–7290.
24 S. Regonda, M. Aryal and W. Hu, *J. Vac. Sci. Technol., B: Microelectron. Nanometer Struct.–Process., Meas., Phenom.*, 2008, **26**(6), 2247–2251.
25 S. Yang, M. Megens, J. Aizenberg, P. Wiltzius, P. M. Chaikin and W. B. Russel, *Chem. Mater.*, 2002, **14**(7), 2831–2833.
26 R. D. Hartschuh, A. Kisliuk, V. Novikov, A. P. Sokolov, P. R. Heyliger, C. M. Flannery, W. L. Johnson, C. L. Soles and W. L. Wu, *Appl. Phys. Lett.*, 2005, **87**, 173121.
27 R. S. Bandhu, R. Sooryakumar and K. Bussmann, *Ann. Phys.*, 2011, **523**(1–2), 107–120.
28 R. J. Jiménez Riobóo, A. Sánchez-Sánchez and C. Prieto, *Phys. Rev. B: Condens. Matter*, 2016, **94**, 014313.
29 D. Yudistira, A. Boes, B. Graczykowski, F. Alzina, L. Y. Yeo, C. M. Sotomayor Torres and A. Mitchell, *Phys. Rev. B: Condens. Matter*, 2016, **94**, 094304.
30 F. T. Arechhi and E. O. Schulz-Dubois, *Laser Handbook*, North-Holland, 1972.
31 D. Royer and E. Dieulesaint, *Elastic Waves in Solids*, Springer, 2010.
32 A. M. Rakhymzhanov, A. Gueddida, E. Alonso-Redondo, Z. N. Utegulov, D. Perevoznik, K. Kurselis, B. N. Chichkov, E. H. E. Boudouti, B. Djafari-Rouhani and G. Fytas, *Appl. Phys. Lett.*, 2016, **108**, 201901.
33 S. J. Tucker, B. Fu, S. Kar, S. Heinz and J. S. Wiggins, *Composites, Part A*, 2010, **41**, 1441–1446.
34 G. Stan, C. V. Ciobanu, I. Levin, H. J. Yoo, A. Myers, K. Singh, C. Jezewski, B. Miner and S. W. King, *Nano Lett.*, 2015, **15**(6), 3845–3850.
35 K. J. Alvine, Y. Ding, J. F. Douglas, H. W. Ro, B. C. Okerberg, A. Karim and C. L. Soles, *Soft Matter*, 2009, **5**(15), 2913.
36 C. Ishiyama and Y. Higo, *J. Polym. Sci., Part B: Polym. Phys.*, 2002, **40**(5), 460–465.
37 M. H. Abedinnasab and M. I. Hussein, *Wave Motion*, 2013, **50**(3), 374–388.
38 W. L. Johnson, S. A. Kim, R. Geiss, C. M. Flannery, C. L. Soles, C. Wang, C. M. Stafford, W. L. Wu, J. M. Torres, B. D. Vogt and P. R. Heyliger, *Nanotechnology*, 2010, **21**, 75703.
39 J. L. Tan, J. Tien, D. M. Pirone, D. S. Gray, K. Bhadriraju and C. S. Chen, *Proc. Natl. Acad. Sci. U. S. A.*, 2003, **100**(4), 1484–1489.
40 C. W. Higginbotham, M. Cardona and F. H. Pollak, *Phys. Rev.*, 1969, **184**(3), 821–829.
41 S. Rudykh and M. C. Boyce, *Phys. Rev. Lett.*, 2014, **112**(3), 034301.
42 S. Amoudache, Y. Pennec, B. D. Rouhani, A. Khater, R. Lucklum and R. Tigrine, *J. Appl. Phys.*, 2014, **115**(13), 134503.
43 L. Montemayor, V. Chernow and J. R. Greer, *MRS Bull.*, 2015, **40**(12), 1122–1129.
44 B. Davies, A. King, P. Newman, A. Minett, C. R. Dunstan and H. Zreiqat, *Sci. Rep.*, 2014, **4**, 7538.
45 Y. L. Xu, X. G. Tian and C. Q. Chen, *Phys. B*, 2012, **407**(12), 1995–2001.
46 P.-Y. Guerder, A. C. Deymier-Black, N. Z. Swinteck, J. O. Vasseur, O. Bou-Matar, K. Muralidharan and P. A. Deymier, *J. Mech. Behav. Biomed. Mater.*, 2014, **37**, 24–32.